Landscape and Urban Planning 219 (2022) 104316

Contents lists available at ScienceDirect

Landscape and Urban Planning

journal homepage: www.elsevier.com/locate/landurbplan

A global analysis of multifaceted urbanization patterns using Earth Observation data from 1975 to 2015

Yunyu Tian [a,*], Nandin-Erdene Tsendbazar [a], Eveline van Leeuwen [b], Rasmus Fensholt [c], Martin Herold [a]

[a] Laboratory of Geo-information Science and Remote Sensing, Wageningen University & Research, Droevendaalsesteeg 3, 6708 PB Wageningen, the Netherlands
[b] Urban Economics, Wageningen University & Research, Hollandseweg 1, 6706 KN Wageningen, the Netherlands
[c] Department of Geosciences and Natural Resource Management, University of Copenhagen, Øster Voldgade 10, DK-1350 Copenhagen, Denmark

HIGHLIGHTS

- Multifaceted nature of urbanization varies greatly across regions and times.
- Increased population and built-up patch density are dominant in Asia and Africa.
- The major urbanization types in urban, suburban, and rural areas are different.
- Urbanization is less intense, more compact, and 'greener' over the recent decade.

ARTICLE INFO

Keywords:
Built-up expansion
Population change
Greenness loss
Urbanization types
Social–land cover–environment interactions

ABSTRACT

Urbanization as a global phenomenon is a multifaceted process. Here we do the first global attempt to characterize the complexity of urbanization from 1975 to 2015 in terms of population, built-up structure, and greenness per 5 × 5 km^2 grid covering global inhabited areas, using Earth Observation data sources. Our results emphasize the multifaceted nature of urbanization that varies greatly across regions and times, in addition to the steady expansion of built-up land. Increased population density and built-up patch density were the dominant characteristics in Asia and Africa, while urbanization in Europe and North America took a rather steady pace, combined with widespread greening. According to the urbanization types identified by a self-organizing map (SOM) algorithm, a large proportion of urban and suburban areas experienced two dynamic urbanization types – *built-up extension/leapfrog* and *built-up infill with large population increase*. During different historical periods (1975–1990, 1990–2000, and 2000–2015), annual rates of increase in population and built-up density were slowing coinciding with an increasing greenness – signaling that urbanization processes are becoming less intense, more compact, and 'greener' over the most recent period. Our findings facilitate the comprehensive understanding of global urbanization that is a complex process with many local variations and characteristics, and underscore the need for region-based strategies towards sustainable development instead of a 'one-size-fits-all' policy for cities.

1. Introduction

Urbanization as a global phenomenon is multifaceted, varies regionally, and poses a wide range of environmental and social challenges. We define 'multifaceted urbanization' as demographic, physical (land cover/use), and environmental changes, based on previous research (Balk, Nghiem, Jones, Liu, & Dunn, 2019; Shaw, van Vliet, & Verburg, 2020). Over the past 40 years, global population has almost doubled and built-up areas expanded by over 150% in urban regions (Melchiorri et al., 2018; Oecd, 2020). The growth of population and built-up area has caused tremendous pressures on natural resources like residential water use, wood used for industrial purposes, and energy use (Grimm et al., 2008). One of the most significant effects is the loss and degradation of green areas (Kabisch et al., 2016; van Vliet, Eitelberg, & Verburg, 2017), which is known to provide ecosystem services, such as air purification, cooling, and recreation for humans (Chang et al., 2017;

* Corresponding author at: PO Box 47, 6700AA Wageningen, the Netherlands.
E-mail address: yunyu.tian@wur.nl (Y. Tian).

https://doi.org/10.1016/j.landurbplan.2021.104316
Received 21 June 2021; Received in revised form 19 November 2021; Accepted 20 November 2021
Available online 28 November 2021

Table 1
Data sets used in this study.

Objective	Dataset	Spatial resolution	Temporal coverage	Definition	**Source data**
Population	GHS population grid (GHS-POP)	250 m	1975, 1990, 2000, 2015	Population counts per grid	Census data, GHS-BUILT
Built-up	GHS multi-temporal built-up grid (GHS-BUILT)	38 m	1975, 1990, 2000, 2015	Buildings/man-made objects	Landsat/ Sentinel-1
Greenness	Third generation GIMMS NDVI	5 arc minutes	1982 (1982-01-01 to 1982-12-30), 1990 (1988-01-01 to 1991-12-30)	Vegetation cover as well as its condition	AVHRR sensors
	MODIS/Terra monthly NDVI	0.05 degree	2000 (2000-01-01 to 2002-12-30), 2015 (2012-01-01 to 2015-12-30)		MODIS sensors
Urban/suburban/rural classification	GHS settlement grid (GHS-SMOD)	1 km	1975	Urban (high-density clusters); Suburban (low-density clusters); Rural (rural grid cells)	GHS-BUILT, GHS-POP

Wang, Zhou, Pickett, Yu, & Li, 2019). >60% of the reported built-up expansion worldwide from 1970 to 2010 was formerly agricultural land (Güneralp, Reba, Hales, Wentz, & Seto, 2020). With rapid urbanization and its extensive impacts, it is increasingly important to understand urbanization processes in terms of population, built-up land, and greenness towards achieving Sustainable Development Goals in cities (e.g. SDG 11) worldwide (UN-Habitat, 2021).

Satellite-based products provide opportunities for monitoring these urbanization processes across the world and over a long period, particularly for the urban/built-up expansion (Esch et al., 2020; Liu et al., 2019). Although the first generation of global satellite-based maps (e.g. MODIS500, CCI, GlobCover300) has been widely used for urbanization analysis (Grekousis, Mountrakis, & Kavouras, 2015; Potere, Schneider, Angel, & Civco, 2009), their shortfalls were also reported, such as the inability to map fine-scale built-up expansion from coarse resolution (300 m–10 km) and ambiguous definition of the urban or built-up area (Yang, Xiao, Feng, & Li, 2017). Most of these issues are tackled in recent global products with a higher spatial resolution (10 m–50 m), including the 30 m Global Land Cover product (GlobeLand30) (Chen et al., 2015), the Global Human Settlement Layer (GHSL) (Corbane et al., 2019) and the Global Urban Footprint (Esch et al., 2013). Particularly, the GHSL provides a high spatial resolution (38 m) of multi-temporal built-up land based on a clear definition – buildings, which makes it possible to characterize spatial patterns of built-up expansion at the grid level.

Based on recent global satellite data (e.g. GHSL), urbanization has been analyzed in terms of population change (Melchiorri et al., 2018), built-up expansion (Güneralp et al., 2020; Liu et al., 2019) and greenness change (Corbane et al., 2020) individually. However, there is little systematic and comprehensive analysis of these trends, particularly for all the global cities not only the large ones (Sun, Chen, Li, & Huang, 2020). Importantly, dynamics of population – built-up – greenness cannot be simply conceptualized as driver – land change – impact, since their causality is not straightforward (Shaw et al., 2020). For instance, population growth usually leads to built-up expansion (van Vliet, Verburg, Grădinaru, & Hersperger, 2019), but the built-up expansion rate has exceeded the population growth rate globally (Liu et al., 2020). Thus, the 'multifaceted urbanization' concept can help us identify the dominant trend among multi-changes, understand social–land cover–environment interactions deeply, and provide a comprehensive classification for urbanization patterns. However, such multifaceted approach has not been applied at the global scale and long time series, while understanding local dominant trend and urbanization type from a global view is needed for national policies.

Moreover, existing global research has revealed the dramatic uneven urbanization at continental-, national- and city-scale (Güneralp et al., 2020; Sun et al., 2020), leaving out the heterogeneity within cities such as urban-suburban-rural differences. Recently, the GHSL provides a global definition of urban, suburban, and rural areas according to population size and density, which greatly increased the reliability of international comparisons (Oecd, 2020). For example, van Vliet et al. (2019) used this definition to compare the changes in population and built-up density of urban, suburban, and rural areas in Europe. But they are confined to the analysis of pixels that change from non-built-up to built-up land, regardless of changes at the landscape level reflected by the built-up structure (Xu, Zhou, Jiao, & Zhao, 2020). International urban-suburban-rural comparison in urbanization lacks the characterization of built-up structures, which will add a landscape-level understanding to urban-suburban-rural differences that could be useful for region-based land use planning towards sustainable urbanization.

To fill the gaps in assessing and understanding urbanization changes globally, we integrated satellite-based data (the GHSL and NDVI products) of population, built-up density, and structure, and greenness to characterize global multifaceted urbanization at 5 × 5 km^2 grid-level from 1975 to 2015. We further identified the dominant characteristics as well as urbanization types for every inhabited grid. We address two questions: First, how do multifaceted urbanization processes co-occur within inhabited grids, and what are urbanization types across the world? Second, what are the differences in this multifaceted urbanization between inhabited classes (urban, suburban, and rural) and between historical periods (1975–1990, 1990–2000, and 2000–2015)? Our study provides new insights on urbanization with unprecedented spatiotemporal detail, fine-scale, and multi-dimensions. We go beyond past studies of global urbanization that analyze major urbanization processes together for every inhabited grid and develop a comprehensive classification of urbanization patterns for comparing urbanization in urban, suburban, and rural areas, which could be useful for local planning of land use and population across the world.

2. Data and methods

2.1. Data source

Data used in this study are shown in Table 1. The Global Human Settlement Layer (GHSL) released in 2016 (GHS P2016) was used to capture the details in population change and built-up expansion as well as to classify urban-suburban-rural grids. The GHSL contains both built-up and population information for a long-term period (1975–2015) and has been proven to be accurate and reliable for capturing global built-up changes, even in complex urban centers and low-density peri-urban areas (Klotz, Kemper, Geiß, Esch, & Taubenböck, 2016; Leyk, Uhl, Balk, & Jones, 2018). The multi-temporal built-up pixels (GHS-BUILT) describe the presence of built-up area in each epoch, which were extracted from Landsat image archives using a Symbolic Machine Learning approach. More details can be found in Pesaresi and Freire (2016). Freire, Macmanus, Pesaresi, and Doxsey-Whitfield (2016) also disaggregated population censuses from Gridded Population of the World (GPW) into 250 m grids according to built-up information in the GHS-BUILT grids and resulted in population counts per 250 m grid (GHS-POP) which disregards administrative boundaries.

Time-series data of Normalized Difference Vegetation Index (NDVI) were chosen to assess greenness in this study, which is widely used to investigate the responses of greenness to urbanization (Jin, Wang, & Li,

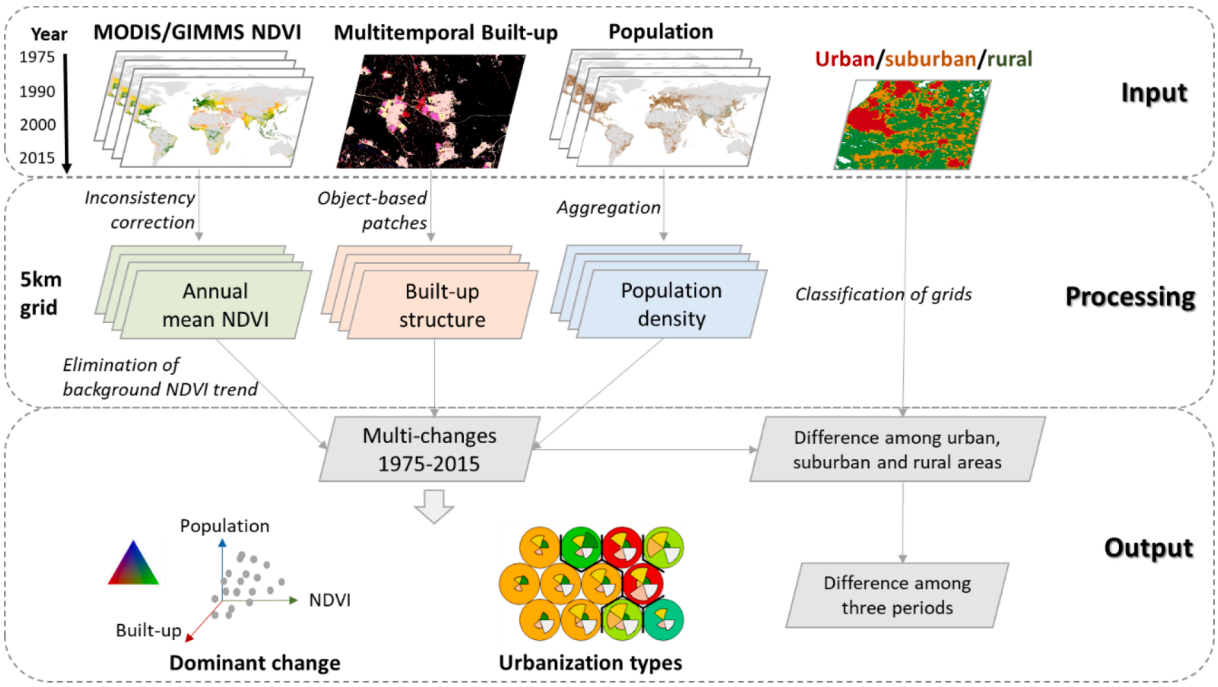

Fig. 1. The conceptual workflow of this study.

2018; Liu et al., 2015). Previous research have demonstrated the reliability of NDVI as a popular proxy to estimate vegetation cover as well as its condition including urban green space (Corbane et al., 2020; Lu, Coops, & Hermosilla, 2017). NDVI is also more sensitive to the changes of vegetation cover in urban context compared to other vegetation indicators such as the Enhanced Vegetation Index (EVI) (Huete, Didan, van Leeuwen, Miura, & Glenn, 2011; Zhang, Friedl, Schaaf, Strahler, & Liu, 2005). Long-term (1982–2015) NDVI series could have been obtained from Advanced Very High-Resolution Radiometer (AVHRR) data or Landsat images. However, MODIS–NDVI performs better than any AVHRR–NDVI data set globally (Beck et al., 2011), and Landsat-NDVI cannot meet the temporal consistency due to different sensors

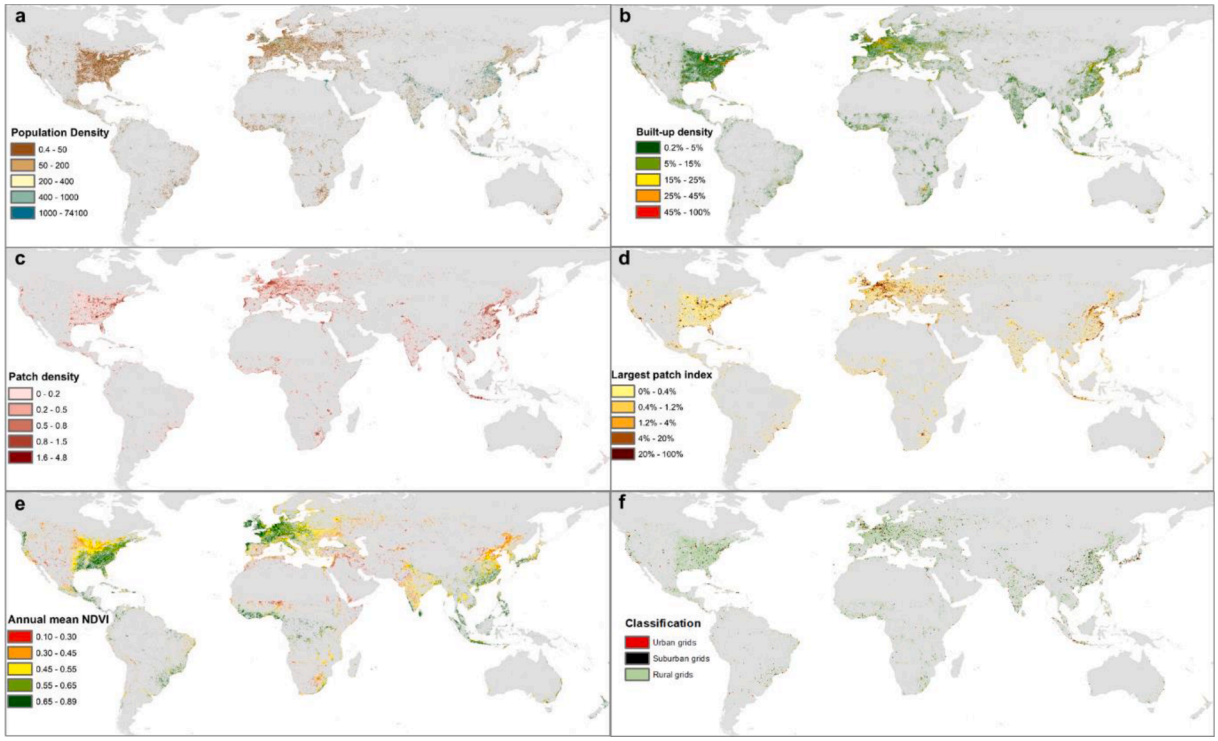

Fig. 2. Multi-characteristics of global inhabited grids in 2015, including population count per km^2 a, the proportion of built-up area within the size of the grid cell b, the number of built-up patches per km^2 c, the proportion of the largest built-up patch area d, and the annual mean NDVI e, as well as urban-suburban-rural classification (https://ghsl.jrc.ec.europa.eu/data.php#GHSLBasics) in 1975f. Some zoom-in snapshots are listed in Fig. A1 and the interactive maps can be accessed at https://qgiscloud.com/tianyunyu/2015/.

(Corbane et al., 2020). Since the MODIS sensor was not launched into earth orbit by NASA until 1999, we combined MODIS/Terra Monthly NDVI products (MOD13C2) for 2000 and 2015 with GIMMS NDVI from AVHRR sensors (NDVI3g) for 1982 and 1990 to attain the long time series (Table 1).

$$Largest\ patch\ index\ (LPI) = \frac{Area\ of\ the\ largest\ built\ -\ up\ patch\ per\ grid\ \left(\mathrm{km}^2\right)}{Area\ of\ grid\ \ \left(25\ \mathrm{km}^2\right)} \times 100\% \quad (2)$$

2.2. Characterizing multifaceted urbanization

In this study, we characterized multifaceted urbanization from 1975 to 2015 within 5 km inhabited grids worldwide. Although most of data were available on a higher spatial resolution, we chose a 5 km resolution because it is a suitable scale for global analysis and minimizes the uncertainty in data sources (e.g. GHS-POP) and inevitable propagation in spatial processing (Liu et al., 2020). In addition, compromised 5 km resolution could reflect the dynamics in landscape patterns based on 38 m built-up pixels and human-environment interactions (Li, van Vliet, Ke, & Verburg, 2019; Malek & Verburg, 2017). The whole workflow (Fig. 1) was operated through the joint use of the Google Earth Engine (GEE) platform and R. More details will be explained in the following sections.

2.2.1. Population density and built-up density

The global 5 km-gridded maps of population density and built-up density were computed for the epoch 1975, 1990, 2000, and 2015. Population count at 250 m resolution (GHS-POP) was spatially aggregated to 5 km resolution by sum. The 5 km-gridded map of population density was created after dividing the population count by the size of the cell (25 km^2). Similarly, we aggregated 38 m built-up pixels into 5 km resolution by computing the proportion of built-up area within the size of the 5 km cell, which is referred to as built-up density in this study. As we focus on urbanization that occurs in inhabited areas, uninhabited grid cells where population equals zero in 2015 were masked out. This extent was applied to the whole study. Finally, we obtained population density and built-up density in global 5 km inhabited grids for the epoch 1975, 1990, 2000, and 2015 (Fig. 2a–b). Changes in population density and built-up density were computed from the difference between layers of epochs.

2.2.2. Metrics for built-up structure

In addition to built-up density, many landscape metrics have been used to quantify built-up structure, including patch numbers, patch density, mean patch size, largest patch index, aggregation index, and so on (Haas, Furberg, & Ban, 2015; Herold, Goldstein, & Clarke, 2003; Zhong, Lin, & Zhou, 2019). Generally, they can be divided into fragmentation and agglomeration indices, and high collinearity exists among similar metrics (Xu et al., 2020; Yu & Ng, 2007). Hence, we chose patch density and the largest patch index to represent fragmentation and compactness of built-up structure, respectively.

First, we identified built-up patches within each 5 km grid for each epoch based on 38 m built-up pixels (GHS-BUILT). The approach used here is the object-based method in GEE. Built-up pixels were assigned by a grid ID representing the grid where 38 m pixels are located, and then connected pixels with the same grid ID were labeled by a unique patch ID. As a result, built-up patches in each grid are sets of unique objects with four-neighbor connectivity of built-up pixels. All pixels belonging to a built-up patch are assigned the same patch ID value. Second, we computed the area of every built-up patch by counting the number of pixels composing the patch and counted the number of built-up patches in each grid using the distinction of patch IDs. Third, we used these statistics of built-up patches to calculate patch density and the largest patch index per grid (e.g. Fig. 2c and d) as follows:

$$Patch\ density\ \ (PD) = \frac{Number\ of\ built\ -\ up\ patches\ per\ grid}{Area\ \ of\ grid\ \left(25\ \mathrm{km}^2\right)} \quad (1)$$

Higher PD means a more fragmented built-up pattern, while higher LPI (i.e. 1) means a more agglomerated built-up pattern with a high built-up density. If the built-up land grows spatially more aggregated around an existing urban core, the LPI increases (Herold et al., 2003). Therefore, built-up expansion can be classified into three modes based on changes in these two metrics: infill, extension, and leapfrog (Xu et al., 2020). Infill expansion is a compact and intensive pattern that normally does not increase the extent, while expansion away from the core built-up area is an extension pattern, and leapfrog is a more discontinuous mode of expansion (Sun, Wu, Lv, Yao, & Wei, 2012; Yu & Zhou, 2017).

2.2.3. Assessment of greenness from satellite data

Global 5 km-gridded maps of annual mean NDVI were calculated for 1982, 1990, 2000, and 2015 (Fig. 2e). First, we collected monthly MODIS-NDVI products during time intervals centered on 2000 and 2015, as well as GIMMS-NDVI centered on 1982 and 1990. The time intervals (as shown in Table 1) were selected to match the epochs of the data collections used to derive the multi-temporal built-up pixels (GHS-BUILT) and to mitigate inter-annual variability and seasonal anomalies that may have affected the greenness change analysis (Corbane et al., 2020). Annual mean NDVI was calculated by the average of monthly NDVI maps within the time interval. Second, to match the GIMMS-NDVI with the MODIS-NDVI record for 1982 and 1990, we applied global gridded maps of regression coefficients (slope and intercept) to the annual mean GIMMS-NDVI map. The regression coefficients were generated by Fensholt and Proud (2012) from the linear regression trend analysis of monthly observations of GIMMS- and MODIS-NDVI overlapping the period from 2000 to 2010. After spatial resampling, we obtained the modified GIMMS-NDVI in 1982 and 1990 as well as the MODIS-NDVI in 2000 and 2015 with temporal consistency at 5 km resolution. Grids that were largely water bodies or bare land (NDVI$<$ 0.1 in 2015) were excluded from this study because perennial water or non-vegetation grids are not interesting for urbanization.

To isolate the urbanization effect on greenness change, we corrected for the background (natural) NDVI change when calculating the NDVI change (Liu et al., 2015). To detect the background NDVI change for every grid (focal grid), we selected grids where built-up density change is lower than 0.01 surrounding a focal grid (5 $\times$ 5 neighborhood) as grids of no urbanization. The background NDVI change of each focal grid was computed by the average of NDVI changes between epochs within its surrounding grids of no urbanization. Finally, the adjusted NDVI change in each focal grid was calculated as its original NDVI change subtracted by its background NDVI change.

2.3. Detection of the dominant change in urbanization

We used RGB synthesized images to display the dominant characteristics (changes) of multifaceted urbanization between 1975 and 2015 per grid cell. Given extreme values in the global map of multi-changes, we first assigned statistical outliers as maximum (Q3)/minimum (Q1) for better visualization. Subsequently, the change values of each

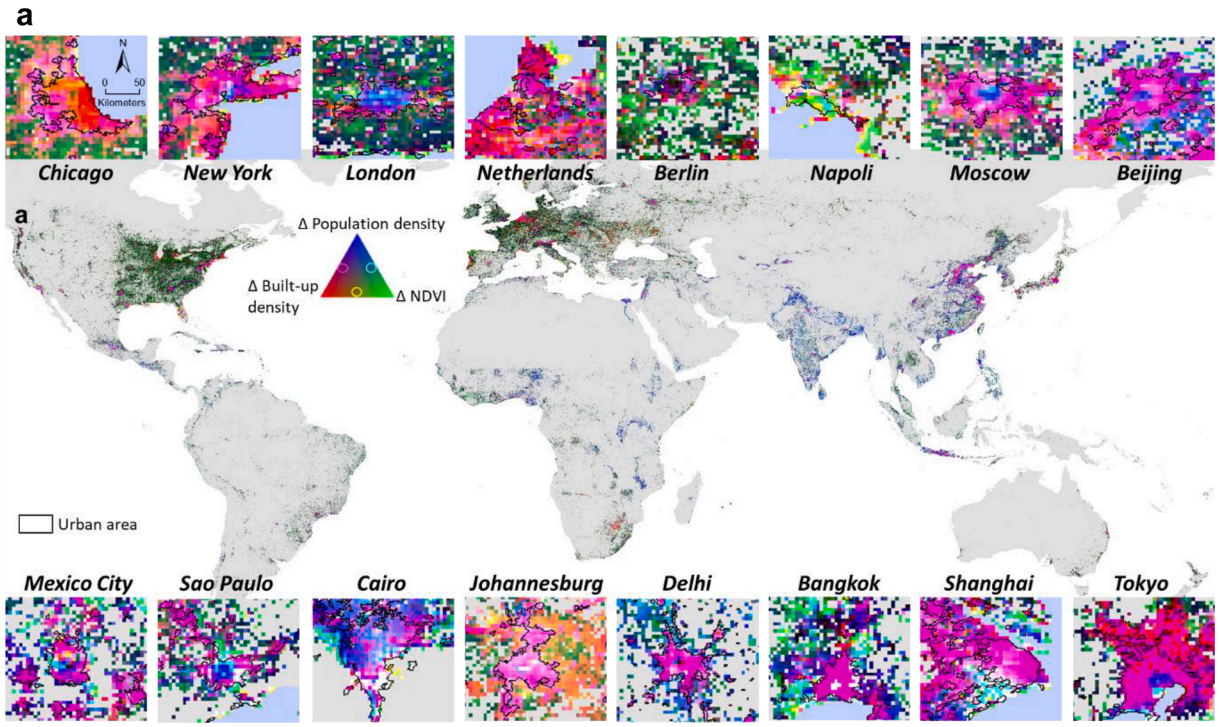

Fig. 4a. Relative dynamics of population density, built-up density, and NDVI from 1975 to 2015. The colors in this figure reveal the dominant increase during the multifaceted urbanization in terms of population change, built-up growth, and greenness change. NDVI denotes greenness in global grids. Examples in the figure reflect the dominant increase in representative global cities as well as the difference between urban and surrounding inhabited grids.

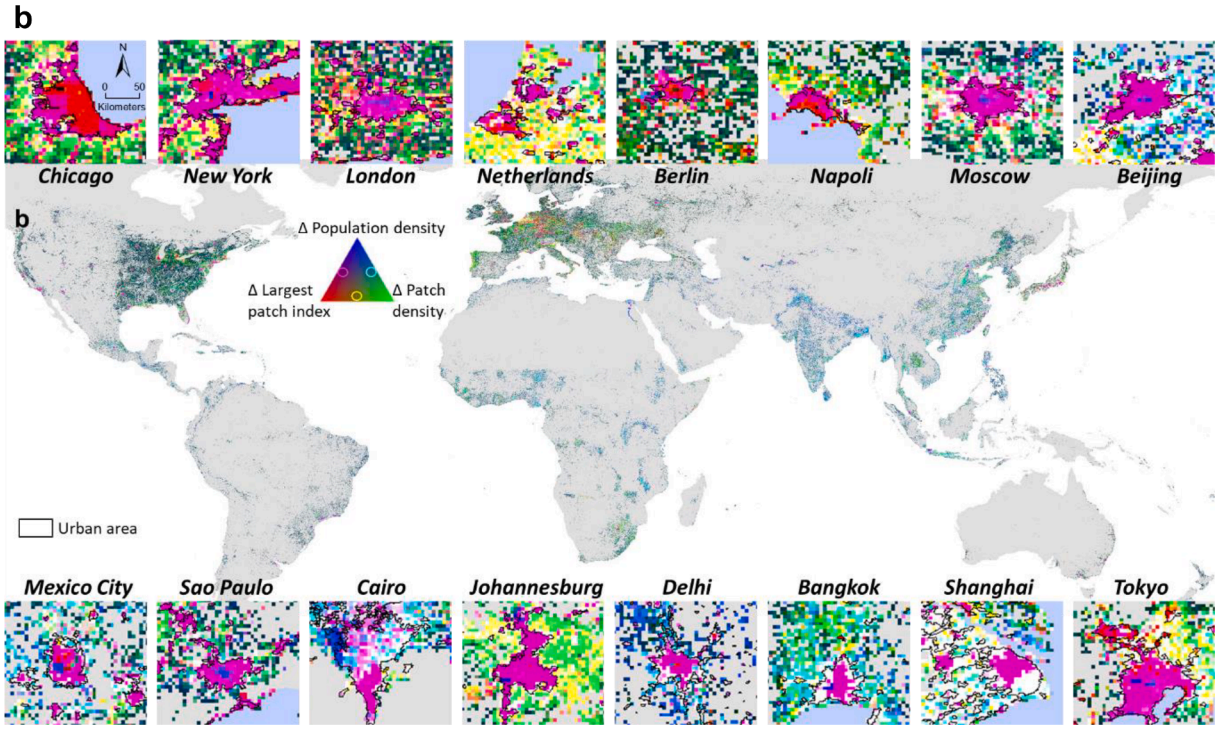

Fig. 4b. Relative dynamics of population density, largest built-up patch index, and built-up patch density from 1975 to 2015. The colors in this figure reveal the dominant increase during the multifaceted urbanization in terms of population change and built-up expansion structure. White color indicates equally high increases in three indicators.

indicator were standardized into 0 to 1 using min–max normalization for global inhabited grids. Two RGB synthesized images were produced by combining standardized changes (i) in population density (blue band), built-up density (red band) and NDVI (green band), and (ii) in population density (blue band), largest built-up patch index (red band) and built-up patch density (green band). The displayed color of a cell represents the relatively large increase among three indicators from a global perspective, which illustrates the dominant characteristics

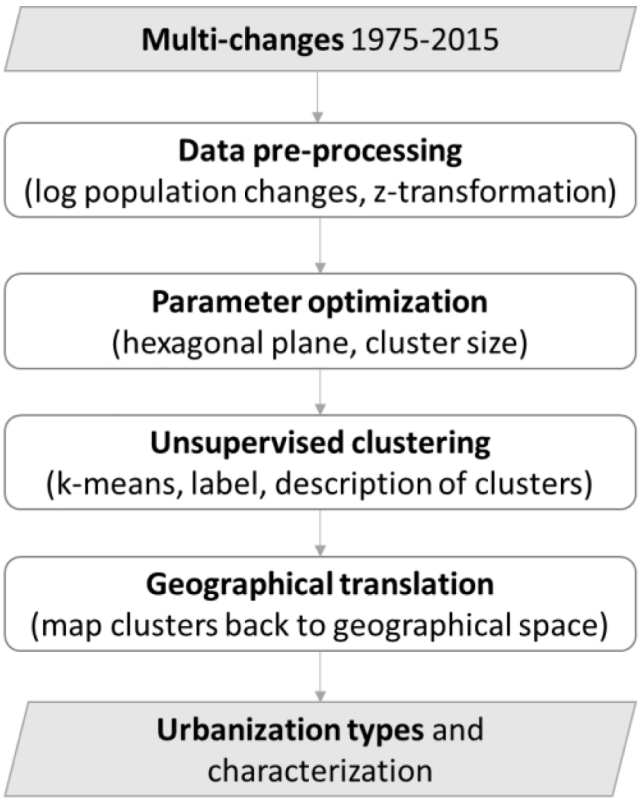

Fig. 3. Workflow of SOM clustering for urbanization types.

(change) of urbanization. Since the three bands of each RGB image are independent, their values can be equally high (close to 1) or low (close to 0) reflected by colors – white or black (Fig. 4a and Fig. 4b).

2.4. Identification of urbanization types

To identify different urbanization types from multifaceted urbanization processes, we adopted a self-organizing map (SOM) algorithm that could automatically cluster grids with similar characteristics of urbanization. In comparison to traditional cluster methods such as k-means or hierarchical clustering, SOM as an unsupervised neural network allows (i) visualizing high-dimensional data by reducing their complexity to fewer (often two) dimensions, (ii) grouping observations (grids in a map) into exclusive sets based on their similarity and (iii) seeing data structure within groups (Levers et al., 2018; Václavík, Lautenbach, Kuemmerle, & Seppelt, 2013). Thus, SOM-based algorithms have been widely applied in geographic and land-system science (Václavík et al., 2013).

The SOM cluster analysis (Fig. 3) was conducted in R version 3.6.1 using the package *kohonen* (Wehrens & Kruisselbrink, 2018). The input data consist of changes in population density, built-up density, patch density, largest patch index, and NDVI between 1975 and 2015, describing the overall increase or decrease of the indicators. First, we z-transformed the five changes to zero mean and unit standard deviation to make indicators comparable. Before the z-transformation, changes in population density were dispersed by a logarithm function separated by different directions (negative and positive numbers) due to the skewed distribution. Z-score normalization allows the results to be interpreted in terms of how much and in which direction the indicator deviates from the global average. Second, we selected a 3 by 4 hexagonal plane and 5 clusters for the SOM model using 50,000 random samples. Typically, a hexagonal plane is preferred since each node has 6 immediate neighbors. We based our dimensionality on a sensitivity analysis that compared varying sizes ranging from 2 by 2 to 6 by 5. The optimal number of clusters was determined by the elbow method which is a key step to generate a meaningful cluster map. Third, an iterative self-organizing process was run to cluster samples and a cluster value was assigned for each record of its closest sample point. Lastly, we mapped the cluster values to the geographical space for all the grids to get the global 5 km-gridded map of urbanization types. The non-normalized values of urbanization indicators within each type are displayed in Fig. A2 (Appendix).

2.5. Urban-suburban-rural classification

We relied on the GHS-SMOD raster dataset for the classification of urban, suburban, and rural grids (Table 1). Given the availability of built-up areas (GHS-BUILT) and population grids (GHS-POP), GHS-SMOD classifies settlements into three main typologies ('high density clusters', 'low density clusters', and 'rural grid cells') at a spatial resolution of 1 km, by porting the rules in the Degree of Urbanization classification (Dijkstra & Poelman, 2014). In the GHS-SMOD representation, the 'high density clusters' are the spatial generalization of contiguous population grids (4-connectivity, gap-filling) with a density of at least 1500 inhabitants per km2 or a density of built-up surface over 50%, and a minimum total resident population of 50000. The 'low density clusters' are continuous grids with a density of at least 300 inhabitants per km2 and a minimum total population of 5000. The 'rural grid cells' are grids outside 'high density clusters' and 'low density clusters' with population density of less than 300. This classification can be used to define urban, suburban, and rural grids since it integrates population distribution and built-up density which makes it rational to be applied universally. More details can be found at https://ghsl.jrc.ec.europa.eu/data.php#GHSLBasics, and examples are presented in Fig. A1. Therefore, we translated SMOD classes to urban, suburban, and rural classes.

The GHS-SMOD raster dataset in 1975 was used to classify the inhabited grids because we are interested in the urbanization dynamics from 1975 to 2015. Given some inhabited grids in 2015 were uninhabited (no population) in 1975, we classified these grids as the rural class for this study. To match the 5 km grids, we aggregated the GHS-SMOD at 1 km resolution to 5 km resolution by the majority rule (Fig. 2f). The final urban-suburban-rural classification was adopted to explore urban-suburban-rural differences in urbanization types (Fig. 6). In addition to the absolute changes per grid we analyzed in this study, relative changes compared to the initial values in 1975 and total changes of population and built-up land were computed for urban, suburban, and rural areas across periods (Fig. 8).

3. Results

3.1. Multifaceted urbanization between 1975 and 2015

From the global average change of 5 km inhabited grids, it can be observed that the population density is increased by 169 persons per km^2 and built-up density by 4% but NDVI value decreased by 0.01 from 1975 to 2015. When looking at multifaceted urbanization, we found that the dominant change varied greatly across regions (Fig. 4a and Fig. 4b). America and Europe are mostly greenish (Fig. 4a), indicating that increased or negligibly decreased greenness dominated most inhabited grids, except for some urban cores. In contrast, blue areas are mainly visible in Asia and Africa, which indicates increased population density as the dominant change (Fig. 4a). Furthermore, when investigating changes of built-up structure and population (Fig. 4b), we found increases in both patch density and population density to be prevalent in Asia and Africa (sky blue areas in Fig. 4b).

Different spatial patterns also evolved in global large cities (example maps in Fig. 4a and Fig. 4b). In urban areas of large cities, urbanization was mostly dominated by both built-up expansion and population growth (pink areas in Fig. 4a), and the built-up expansion typically

Table 2
Characteristics of urbanization types from SOM cluster analysis, and statistics for types. The numbers refer to the median values of non-normalized indicators in each urbanization type. The + and − signs represent whether the change is above or below global average change (+is up to 0.25–0.5 s.d., ++ is 0.5–1 s.d., +++ is > 1 s.d.).

SOM urbanization types and Description	Δ Population density (PopD)	Δ Built-up density (BuiD)	Δ Patch density (PatD)	Δ Largest patch index (LPI)	Δ NDVI	Area [%]
(1) Greenness loss: largely decreased NDVI and close to global average for other indicators	32.03, +	2%, −	0.12	0.20%	−0.29, −	2
(2) Steady urbanization: close to global average for all indicators	13.05	1%, −	0.08, -	0.08%	0	69
(3) Population decrease: largely decreased PopD and close to global average for other indicators	−40.77, —	2%	0.12	0.48%, +	−0.01	12
(4) Built-up extension/leapfrog: largely increased PopD, BuiD, PatD, and LPI	220.09, ++	10%, ++	0.56, +++	3.28%, +++	−0.02	17
(5) Built-up infill with large population increase: largely increased PopD, BuiD and LPI but largely decreased PatD	899.07, +++	37%, +++	−0.88, —	44.20%, +++	−0.05, -	1

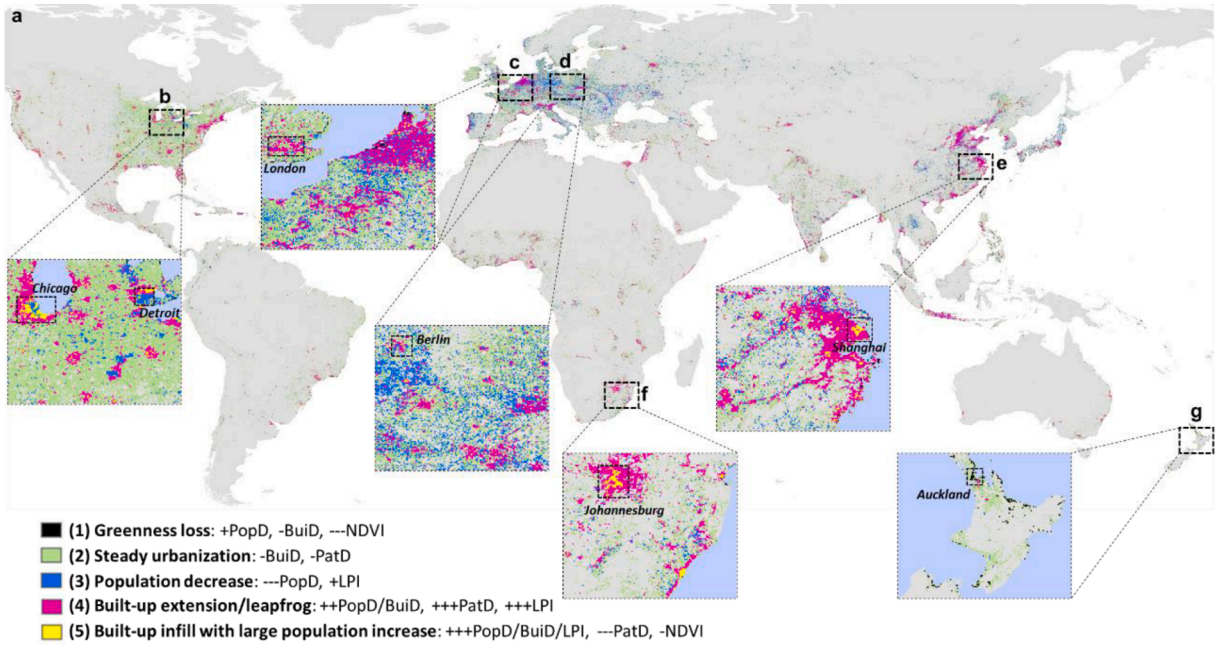

Fig. 5. Global map of urbanization types a, as well as spatial patterns in Eastern America b, Western Europe c, Central Europe d, Eastern China e, and South Africa f. This figure presents the spatial distribution of five urbanization types we identified based on changes in population, built-up, and NDVI. Dashed boxes within example maps (b-f) mark out the urban area of some large cities.

manifested as the increase of the largest patch index (pink areas in Fig. 4b). Nevertheless, there were some exceptions of the dominant change in Europe's urban areas (Fig. 4a), such as population growth (blue areas) in London, increase or negligible decrease in greenness (green areas) in Napoli, and small increases in all indicators (dark areas) in Berlin. At the heart of some megacities such as Tokyo, Beijing and Moscow, population growth played the only dominant role (blue areas in Fig. 4a). In contrast to the relatively parallel pattern in urban areas, larger regional differences existed in surrounding non-urban areas, displayed as more varying colors in Fig. 4a and Fig. 4b. For instance,

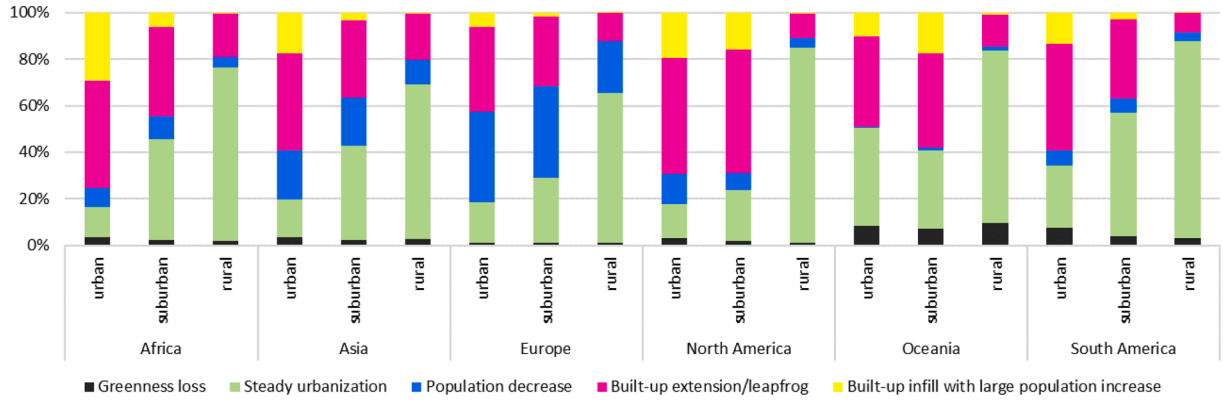

Fig. 6. Continental summaries for the five urbanization types in urban, suburban, and rural grids. Grids of urbanization types were counted for North America (N. Amer.), South America (S. Amer.), Europe, Africa, Asia, and Oceania (which contains Australia).

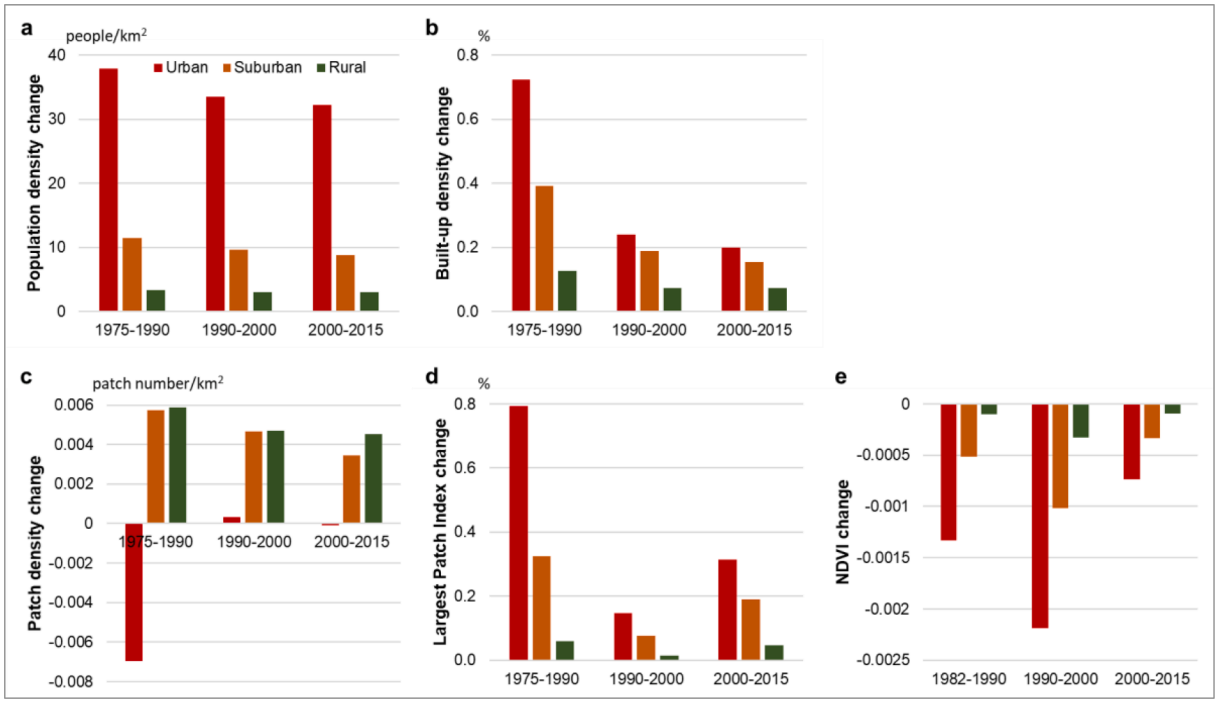

Fig. 7. Average annual changes per urban, suburban, and rural grid cell during different periods (1975–1990, 1990–2000, 2000–2015). Patch density and the largest patch index refer to built-up patches within inhabited grids.

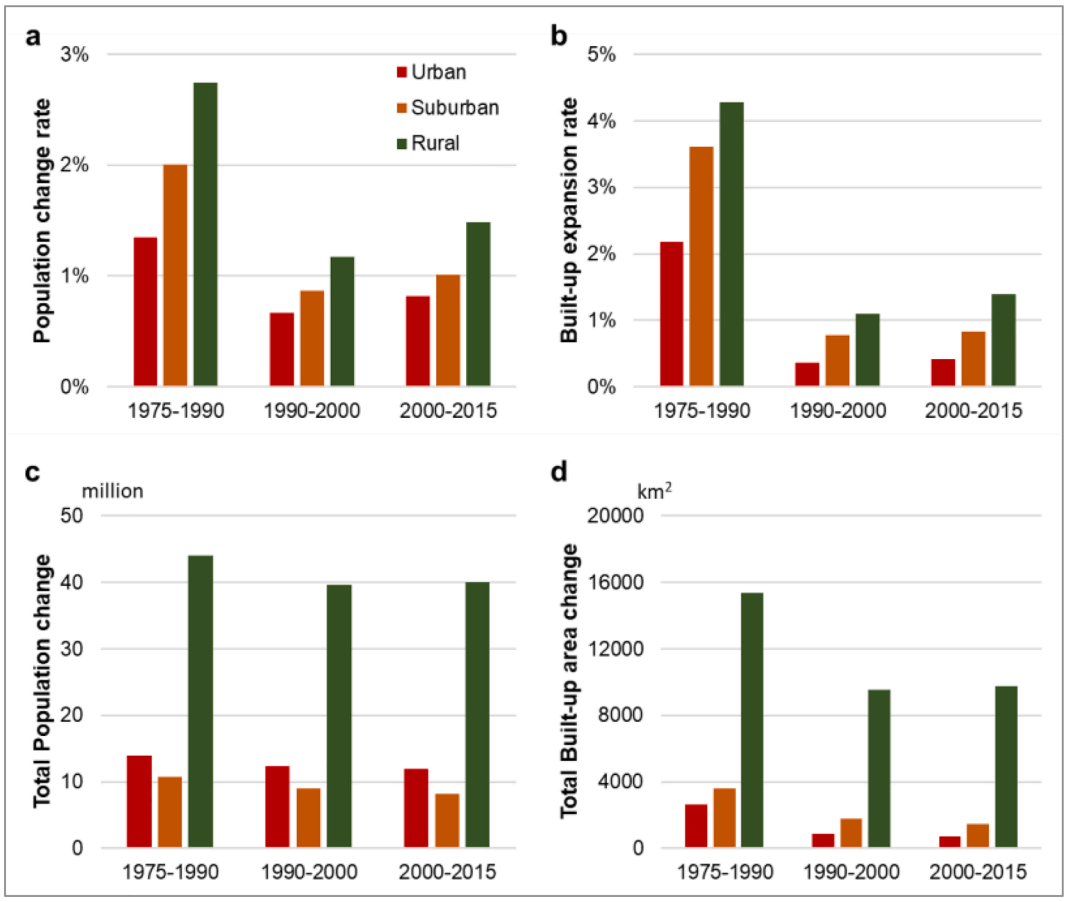

Fig. 8. Annual relative changes a-b and absolute changes c-d in all urban, suburban, and rural grid cells during different periods.

increased or negligibly decreased greenness was evident in New York, London and Berlin (green areas in Fig. 4a), while the growth of population and built-up areas was dominant in Shanghai and Beijing (pink areas in Fig. 4a), and built-up expansion played a vital role in the Netherlands and Chicago (red areas in Fig. 4a).

3.2. Urbanization types

In the next step, we further classified the multifaceted urbanization into five urbanization types using the SOM algorithm (Table 2; Fig. A2). Globally, *steady urbanization* was the major type covering almost 70% of global inhabited grids, representing a continuing urbanization trend in mainly non-urban regions. The urbanization types showed some distinct patterns across regions (Fig. 5). *Steady urbanization* mostly occurred in America, Europe, and India (Fig. 5a), and was primarily found in rural areas of America and India but both in urban and rural areas of Europe such as London and Paris (Fig. 5c). *Built-up extension/leapfrog* was not only found in surrounding areas of city centers globally (Fig. 5a) but was also particularly widespread in Eastern China, Java, and in almost the whole of the Netherlands (e.g. Fig. 5a, c). *Population decrease* primarily occurred in Europe such as Portugal, Germany and Poland (e.g. Fig. 5d), covering 24% of inhabited grids in Europe. This type was also found in urban areas of North America even in some large cities like Chicago and Detroit (Fig. 5b). *Greenness loss* mostly occurred in coastal areas, especially in Oceania such as New Zealand (Fig. 5g). *Built-up infill with large population increase* covers only about 1% of global inhabited grids, but it represents the most substantial urbanization with the highest increases of population and built-up density among the five types. It was typically found in megacities such as Chicago, Shanghai and Johannesburg (Fig. 5b, e, f).

3.3. Urban-suburban-rural differences

According to the proportions of urbanization types (Fig. 6), the main urban-suburban-rural difference was that *steady urbanization* is the major type in rural areas across all continents (>60%), while the two dynamic urbanization types – *built-up extension/leapfrog* and *built-up infill with large population increase* occur in a large portion of urban and suburban areas. Particularly, *built-up infill with large population increase* almost only occurred in urban and suburban grids. Moreover, the major type in urban and suburban areas varies by continent. For urban grids, *built-up extension/leapfrog* was the major type (>30%) in most continents, while *population decrease* dominated in Europe and *steady urbanization* dominated in Oceania. For suburban grids, *steady urbanization* was the major type in South America (53%), Africa (43%), and Asia (40%), while *built-up extension/leapfrog* was leading in North America (53%) and Oceania (40%), and *population decrease* (39%) in Europe. It is interesting to note that in addition to the case of *population decrease* in Europe, this type was noticeable in Asia's suburban grids (21%).

3.4. Difference between historical periods

Three periods were divided based on the available epochs of the data source (GHSL), and we used annual changes to make them comparable. Globally, the absolute increases (Fig. 7a–b) and relative increases (Fig. 8a–b) in population and built-up density have been generally declining in urban, suburban, and rural areas over the three periods. First, the annual growth of population density was slightly declining during three periods globally (Fig. 7a), yet in Africa, the annual growth of population density was rising in urban, suburban and rural areas over three periods (Fig. A3). Second, built-up expansion was slowing (Fig. 7b; Fig. 8b,d) and becoming more compact recently (Fig. 7c–d). During the first period (1975–1990), the annual growth rate of built-up density was nearly twice as fast as the recent two periods, and it mainly occurred in urban areas as infilling with largely decreased patch density (-0.007 patches per km^2 yr^{-1}). In the recent two periods, while the annual growth rates of built-up density were similar, the annual increase in the largest patch index was increasing suggesting a more compact expansion form (Fig. 7b,d).

As for the greenness loss, we found a discontinuous trend during three periods globally (Fig. 7e). First, the annual rate of decrease in greenness during the second period (1990–2000) was much greater than that in the other two periods, accompanied by the smallest annual increase in the largest patch index during 1990–2000. Second, the annual rate of decrease in greenness from 2000 to 2015 was less than that in previous periods. Moreover, a dramatic continental difference exists in greenness loss (Fig. A3). In urban areas, larger greenness loss occurred in Oceania and North America from 1975 to 2000, but greenness loss in Asia and Africa began to exceed them since 2000. Greenness loss in Europe was always the smallest among continents for urban and suburban areas since 1990.

4. Discussion

4.1. Multifaceted urbanization

To our knowledge, this study reports the most comprehensive understanding of global long-term urbanization so far by adopting a multifaceted approach. Our results show that the population density, built-up density, built-up patch density, and the largest built-up patch index were increasing from 1975 to 2015 globally, which are in line with previous global studies of single facet (Güneralp et al., 2020; Liu et al., 2019; Melchiorri et al., 2018). Previous research also found that NDVI was increasing in most global cities between 1990 and 2014 (Corbane et al., 2020), mainly due to global warming and carbon emissions (Zhao, Dai, & Dong, 2018). However, our study reveals that urbanization-related greenness has been decreasing globally (Table 2; Fig. 7e). This discrepancy can be explained by the fact that we aimed to investigate only urbanization-related greenness change by removing background (natural) NDVI trends that could be related to climate change in general (Zhang et al., 2021).

In addition to the global trends, our results emphasize the large regional variation in multifaceted urbanization. Asia and Africa were mostly influenced by high-density urbanization (dominated by increased population and built-up density), while urbanization in Europe and America took a steadier pace, widespread inhabited areas and showed greening (dominated by increased or negligibly decreased NDVI) (Fig. 4a and Fig. 4b). Our urbanization types also reveal an interesting regional variation of urbanization types that deviate from the global average trend. One such type is *population decrease* which represents slow urbanization or counter-urbanization, mostly distributed in Europe (Fig. 5a). Such population decrease in Europe has been confirmed from previous studies (Shaw et al., 2020), which might be due to aging populations and lower fertility rates (Franklin & van Leeuwen, 2018). Surprisingly, it also occurred in many grids of Asia, which might be explained by the large-scale migration from rural to urban areas and from small cities to megacities (Li et al., 2019).

By integrating multifaceted changes, previous global studies reveal that the built-up expansion rate has exceeded the population growth rate globally (e.g. Liu et al., 2020). We integrated more facets than past studies and found that despite the global declining trend, urbanization-related greenness increased in some inhabited grids where the built-up area and population grew (Fig. 4a). This finding adds a new sight into the effects of urbanization on greenness, since many studies showed largely decreased greenness caused by the built-up expansion on cropland or forest areas (Liu et al., 2015; van Vliet et al., 2017). Increased greenness we found could be related to the urban heat island which may prolong the growing season in some regions (Du et al., 2019) and new green spaces such as parks and urban gardens that urbanization often bring along especially in dry and arid regions (Corbane et al., 2020).

4.2. Differences between urban-suburban-rural areas and historical periods

Despite the existing knowledge that denser built-up and population growth in urban grids than in rural grids (Li et al., 2019; Melchiorri et al., 2018), our study elaborates that urban-suburban-rural differences largely vary by continent. First, urbanization in urban areas appeared to be greater than that in suburban areas of South America, Africa and Asia, but urbanization in suburban areas was similar or even greater than that in urban areas of North America, Europe and Oceania, according to the proportion of dynamic urbanization types (Fig. 6). Second, for rural areas, in addition to the *steady urbanization*, *built-up extension/leapfrog* was found in a remarkable portion of Asia and Africa (Fig. 6). This can be explained by built-up fragmentations caused by increasing road networks which might be a driver of urbanization in the countryside.

Furthermore, we found that the relative increases and total increases in villages far exceeded those in urban centers (Fig. 8). In particular, the total built-up area and population grew more greatly in rural areas than urban areas due to the considerably higher number of rural grid cells compared to urban centers. This finding differs from the normal knowledge that the population mainly grows in urban areas (United Nations. (2018), 2018) and can be explained by the large transformation from rural settlements to urban settlements during 1975–2015 (Fig. A4). Thus, while urban areas have usually been the focus of previous urbanization research, the interaction with suburban and rural areas makes an interesting addition to exploring the diverse multifaceted urbanization worldwide.

Many existing studies imply a rapidly increasing urbanization (Güneralp et al., 2020; United Nations. (2018), 2018), but our study provides powerful evidence that urbanization processes are becoming less intense, more compact and more 'green' over the most recent period (2000–2015). We found that the built-up expansion became more compact accompanying the decreasing loss of greenness, according to the comparison of the recent two periods (Fig. 7). Considering our adjusted NDVI change as the urbanization-related change, this result could suggest that the adverse effects of urbanization on vegetation might gradually diminish as the urbanization turns to a built-up aggregation (compacting) stage (Du et al., 2019; Liu et al., 2015). Therefore, global inhabited areas might become 'greener' with stabilizing and sustainable (e.g. compacting built-up expansion) urbanization in the future.

4.3. Uncertainties and limitations

Although the GHSL dataset is the best option for monitoring long-term built-up expansion globally, the identification of built-up land in rural areas is less accurate than in urban areas (Klotz et al., 2016; Leyk et al., 2018). Built-up land in rural areas is scattered and rare, making the previous global land cover products (e.g. CCI-LC and MOD500) almost entirely neglected small settlements within cropland. Until 2016, the GHSL captured built-up land (manmade roofs) in rural areas at 38 m resolution with temporal consistency (1975–1990-2000–2015), but there still exist potential risks of overestimating settlement area in rural regions (Klotz et al., 2016; Sabo et al., 2018). Multi-temporal and refined global maps for the built-up land are needed for improving the accuracy of monitoring built-up expansion in rural areas.

Similar to other global gridded population products, the GHS-POP we used was mainly disaggregated from census data and distributed proportionally over built-up density. Yet, functional use of buildings and their height were not considered in the disaggregation process (Freire et al., 2016), which could cause uncertainties in gridded population of a single epoch. Since those features of existing buildings normally don't change over time, population changes of grid cells with small built-up expansion (urbanization type 1–3) would not be affected by the uncertainties in GHS-POP. Population increase might be underestimated for those expanded land with new high-rise buildings, but population increases in urban areas and type 4–5 are already higher than others (Table 2; Fig. 7). Thus, our conclusions of urbanization types and urban–rural differences in population changes are still valid. By including more building information of the world, more feasible gridded population change can be produced. As for the greenness, we used GIMMS-NDVI in 1982 to represent the greenness in 1975, which is the best option for long-term consistency. We also mitigated the limitation of this temporal deviation by using annual change rates for the comparison between different historical periods.

Future research could explore global multifaceted urbanization by using diverse indicators and methods to provide more comprehensive information for policymakers. For example, the spatial structure of built-up land can be further assessed from monocentric to polycentric (Agyemang, Silva, & Poku-Boansi, 2019). Since our study aims to quantify major urbanization characteristics, we only recognized the dominant increase among multi-changes. The dominant process may be a declining factor such as greenness loss. Moreover, this study mainly analyzed absolute changes per grid due to that many inhabited areas in 2015 were uninhabited in 1975, yet the relative changes might lead to a different urbanization type and spatial pattern. As for the spatial resolution, we compromised it to 5 km due to the original resolution and uncertainties of data sources. Since more data are available at higher resolution in the recent period, urbanization at a higher resolution (e.g. 1–2 km) could be done to better reflect spatial details of changes in built-up structure, population, and greenness at a neighborhood scale.

4.4. Implications for urban development

Investigating grid-level urbanization as a multifaceted process can provide global insights for policymakers towards tailored local strategies. First, our findings of the dominant change detect the major land or social pressures from urbanization of which decision-makers should be aware. For example, many regions in Asia and Africa are particularly sensitive to increases in built-up patch density and population density, since these increases were already prevalent there. Second, our grid-level results highlight the heterogeneity within cities, which can be used in the grid management of cities. For instance, in the urban core of Chicago, some grids are dominated by built-up expansion or population growth while some by increased greenness. Third, our urbanization types based on long-term observation can help governments and international researchers identify the continuing unhealthy regions.

Our exploration of multifaceted urbanization casts an in-depth consideration of healthy and sustainable development for urban planners and researchers. From the demographic perspective, we observed a relatively unsustainable type that is *population decrease*, indicating the 'right-hand' challenges for developed regions and seriously unbalanced urbanization in developing regions. Urban researchers should rethink what can drive urbanization except for the population growth since we revealed that population decrease and built-up expansion co-occurred in many regions of Europe. From the land-use perspective, our findings in urbanization-related greenness could further indicate the location of healthy or unhealthy built-up expansion. The healthy development that built-up expansion and greenness co-increasing in some grids can be studied as a model of urban expansion. In particular, our results on landscape indicators suggest that a compacting form would mitigate greenness loss during built-up expansion, and thus, land-use planning could further focus on the regions with *built-up extension/leapfrog*.

5. Conclusions

To enhance the comprehensive understanding of global multifaceted urbanization from 1975 to 2015, this study analyzed changes in population, built-up structure, and greenness per 5×5 km^2 grid covering global inhabited areas. Results show that Asia and Africa mainly experienced high-density urbanization, while urbanization in Europe and America appeared rather steady, widespread, and showed greening

except for some urban cores. The urbanization types further reveal diverse patterns across continents (e.g. *population decrease* occurred in a large portion of Europe and *built-up extension/leapfrog* in Asia). Urbanization in urban and suburban areas shows a large proportion of two dynamic types – *built-up extension/leapfrog* and *built-up infill with large population increase* while most rural areas experienced a steady, rather low intensity urbanizing. Urbanization processes are becoming less intense, more compact, and 'greener' over the most recent decade, suggesting that the adverse effects of urbanization on vegetation might gradually diminish over time due to more sustainable built-up expansion. Results from this study offer a comprehensive understanding of global multifaceted urbanization particularly in suburban and rural areas and provide valuable insights for region-based policies to mitigate urbanization effects on the environment towards future sustainable development.

Declaration of Competing Interest

The authors declare that they have no known competing financial interests or personal relationships that could have appeared to influence the work reported in this paper.

Acknowledgement

This project is funded by the China Scholarship Council (NO. 201904910503).

Appendix

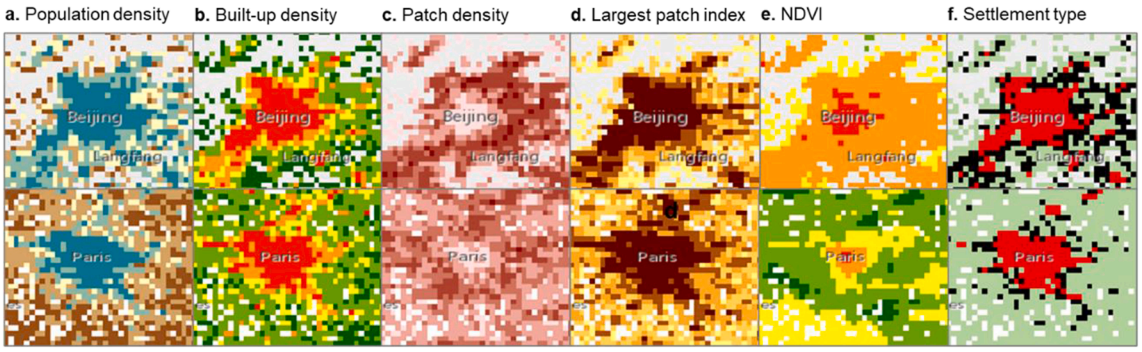

Fig. A1. Zoom-in snapshots of urbanization indicators and settlement types in 2015. Corresponding legends can be found in Fig. 2.

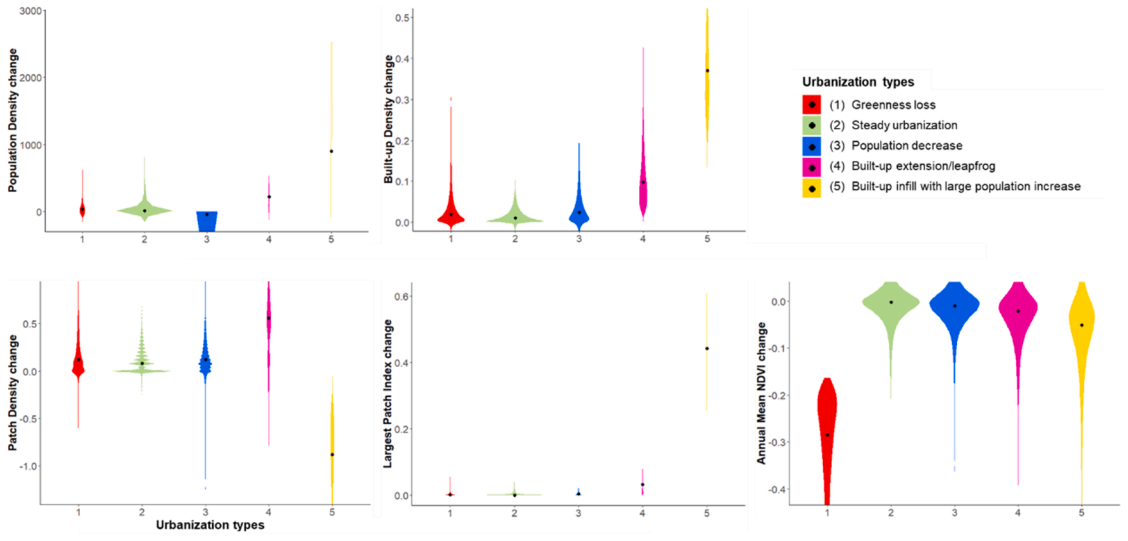

Fig. A2. Violin plots of the data distribution in each urbanization type. The Y-axis is the non-normalized value of urbanization indicators. The dark spot denotes the median value of each type.

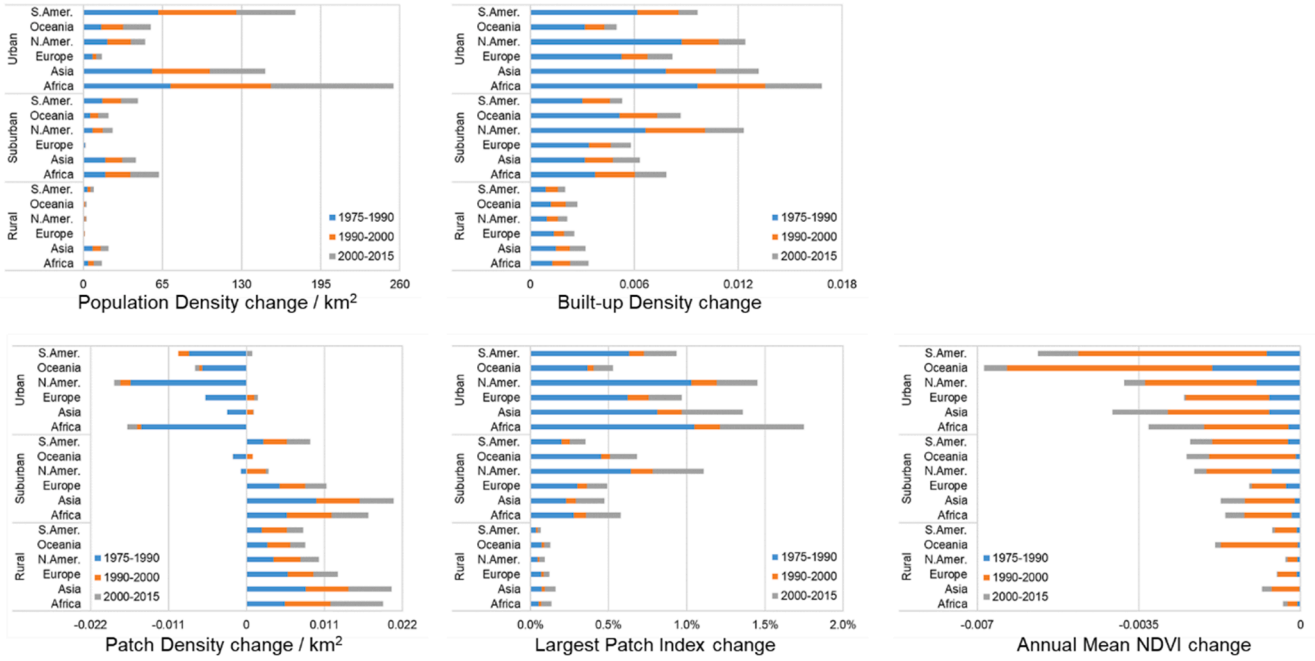

Fig. A3. Annual changes in different periods (1975–1990, 1990–2000, 2000–2015) across continents.

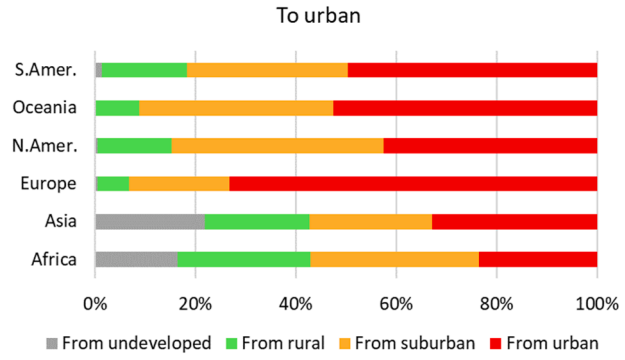

Fig. A4. Transformation from settlement types in 1975 to the urban settlement in 2015 across continents.

References

Agyemang, F. S. K., Silva, E., & Poku-Boansi, M. (2019). Understanding the urban spatial structure of Sub-Saharan African cities using the case of urban development patterns of a Ghanaian city-region. *Habitat International, 85*(December 2018), 21–33. https://doi.org/10.1016/j.habitatint.2019.02.001

Balk, D. L., Nghiem, S. V., Jones, B. R., Liu, Z., & Dunn, G. (2019). Up and out: A multifaceted approach to characterizing urbanization in Greater Saigon, 2000–2009. *Landscape and Urban Planning*. https://doi.org/10.1016/j.landurbplan.2018.07.009

Beck, H. E., Mcvicar, T. R., Van Dijk, A. I. J. M., Schellekens, J., De Jeu, R. A. M., & Bruijnzeel, L. A. (2011). Global evaluation of four AVHRR – NDVI data sets : Intercomparison and assessment against Landsat imagery. *Remote Sensing of Environment, 115*(10), 2547–2563. https://doi.org/10.1016/j.rse.2011.05.012

Chang, J., Qu, Z., Xu, R., Pan, K., Xu, B., Min, Y., … Ge, Y. (2017). Assessing the ecosystem services provided by urban green spaces along urban center-edge gradients. *Scientific Reports*. https://doi.org/10.1038/s41598-017-11559-5

Chen, J., Chen, J., Liao, A., Cao, X., Chen, L., Chen, X., … Mills, J. (2015). Global land cover mapping at 30 m resolution: A POK-based operational approach. *ISPRS Journal of Photogrammetry and Remote Sensing*. https://doi.org/10.1016/j.isprsjprs.2014.09.002

Corbane, C., Martino, P., Panagiotis, P., Aneta, F. J., Michele, M., Sergio, F., … Gustavo, N. (2020). The grey-green divide : Multi-temporal analysis of greenness across 10, 000 urban centres derived from the Global Human Settlement Layer (GHSL). *International Journal of Digital Earth ISSN, 8947*. https://doi.org/10.1080/17538947.2018.1530311

Corbane, C., Pesaresi, M., Kemper, T., Politis, P., Florczyk, A. J., Syrris, V., … Soille, P. (2019). Automated global delineation of human settlements from 40 years of Landsat satellite data archives. *Big Earth Data, 3*(2), 140–169. https://doi.org/10.1080/20964471.2019.1625528

Dijkstra, L., & Poelman, H. (2014). A harmonised definition of cities and rural areas: the new degree of urbanisation. *Regional and Urban Policy*, (June), 28. Retrieved from <http://ec.europa.eu/regional_policy/sources/docgener/work/2014_01_new_urban.pdf>.

Du, J., Fu, Q., Fang, S., Wu, J., He, P., & Quan, Z. (2019). Effects of rapid urbanization on vegetation cover in the metropolises of China over the last four decades. *Ecological Indicators, 107*(July), Article 105458. https://doi.org/10.1016/j.ecolind.2019.105458

Esch, T., Asamer, H., Bachofer, F., Balhar, J., Boettcher, M., Boissier, E., … Zeidler, J. N. (2020). Digital world meets urban planet–new prospects for evidence-based urban studies arising from joint exploitation of big earth data, information technology and shared knowledge. *International Journal of Digital Earth*. https://doi.org/10.1080/17538947.2018.1548655

Esch, T., Marconcini, M., Felbier, A., Roth, A., Heldens, W., Huber, M., … Dech, S. (2013). Urban footprint processor-Fully automated processing chain generating settlement masks from global data of the TanDEM-X mission. *IEEE Geoscience and Remote Sensing Letters*. https://doi.org/10.1109/LGRS.2013.2272953

Fensholt, R., & Proud, S. R. (2012). Evaluation of Earth Observation based global long term vegetation trends — Comparing GIMMS and MODIS global NDVI time series. *Remote Sensing of Environment, 119*, 131–147. https://doi.org/10.1016/j.rse.2011.12.015

Franklin, R. S., & van Leeuwen, E. S. (2018). For Whom the bells Toll: Alonso and a regional science of decline. *International Regional Science Review, 41*(2), 134–151. https://doi.org/10.1177/0160017616675917

Freire, S., Macmanus, K., Pesaresi, M., & Doxsey-Whitfield, E. (2016). *Development of new open and free multi-temporal global population grids at 250 m resolution Validation of remote sensing derived emergency mapping maps View project Megacities View project*, (June). Retrieved from <https://www.researchgate.net/publication/304625387>.

Grekousis, G., Mountrakis, G., & Kavouras, M. (2015). An overview of 21 global and 43 regional land-cover mapping products. *International Journal of Remote Sensing*. https://doi.org/10.1080/01431161.2015.1093195

Grimm, N. B., Faeth, S. H., Golubiewski, N. E., Redman, C. L., Wu, J., Bai, X., & Briggs, J. M. (2008). Global change and the ecology of cities. *Science, 319*(5864), 756–760. https://doi.org/10.1126/science.1150195

Güneralp, B., Reba, M., Hales, B. U., Wentz, E. A., & Seto, K. C. (2020). Trends in urban land expansion, density, and land transitions from 1970 to 2010: A global synthesis. *Environmental Research Letters, 15*(4). https://doi.org/10.1088/1748-9326/ab6669

Haas, J., Furberg, D., & Ban, Y. (2015). Satellite monitoring of urbanization and environmental impacts—A comparison of Stockholm and Shanghai. *International Journal of Applied Earth Observation and Geoinformation*. https://doi.org/10.1016/j.jag.2014.12.008

Herold, M., Goldstein, N. C., & Clarke, K. C. (2003). The spatiotemporal form of urban growth: Measurement, analysis and modeling. *Remote Sensing of Environment*. https://doi.org/10.1016/S0034-4257(03)00075-0

Huete, A., Didan, K., van Leeuwen, W., Miura, T., & Glenn, E. (2011). MODIS vegetation indices. In *Remote Sensing and Digital Image Processing*. https://doi.org/10.1007/978-1-4419-6749-7_26

Jin, K., Wang, F., & Li, P. (2018). Responses of vegetation cover to environmental change in large cities of China. *Sustainability (Switzerland), 10*(1). https://doi.org/10.3390/su10010270

Kabisch, N., Frantzeskaki, N., Pauleit, S., Naumann, S., Davis, M., Artmann, M., … Bonn, A. (2016). Nature-based solutions to climate change mitigation and adaptation in urban areas: Perspectives on indicators, knowledge gaps, barriers, and opportunities for action. *Ecology and Society*. https://doi.org/10.5751/ES-08373-210239

Klotz, M., Kemper, T., Geiß, C., Esch, T., & Taubenböck, H. (2016). How good is the map? A multi-scale cross-comparison framework for global settlement layers: Evidence from Central Europe. *Remote Sensing of Environment*. https://doi.org/10.1016/j.rse.2016.03.001

Levers, C., Müller, D., Erb, K., Haberl, H., Jepsen, M. R., Metzger, M. J., … Kuemmerle, T. (2018). Archetypical patterns and trajectories of land systems in Europe. *Regional Environmental Change, 18*(3), 715–732. https://doi.org/10.1007/s10113-015-0907-x

Leyk, S., Uhl, J. H., Balk, D., & Jones, B. (2018). Assessing the accuracy of multi-temporal built-up land layers across rural-urban trajectories in the United States. *Remote Sensing of Environment*. https://doi.org/10.1016/j.rse.2017.08.035

Li, M., van Vliet, J., Ke, X., & Verburg, P. H. (2019). Mapping settlement systems in China and their change trajectories between 1990 and 2010. *Habitat International, 94* (September), Article 102069. https://doi.org/10.1016/j.habitatint.2019.102069

Liu, C., Huang, X., Zhu, Z., Chen, H., Tang, X., & Gong, J. (2019). Automatic extraction of built-up area from ZY3 multi-view satellite imagery: Analysis of 45 global cities. *Remote Sensing of Environment*. https://doi.org/10.1016/j.rse.2019.03.033

Liu, H., Gong, P., Wang, J., Clinton, N., Bai, Y., & Liang, S. (2020). Annual dynamics of global land cover and its long-term changes from 1982 to 2015. *Earth System Science Data*. https://doi.org/10.5194/essd-12-1217-2020

Liu, X., Huang, Y., Xu, X., Li, X., Li, X., Ciais, P., … Zeng, Z. (2020). High-spatiotemporal-resolution mapping of global urban change from 1985 to 2015. *Nature Sustainability, 3*(7), 564–570. https://doi.org/10.1038/s41893-020-0521-x

Liu, Y., Wang, Y., Peng, J., Du, Y., Liu, X., Li, S., & Zhang, D. (2015). Correlations between urbanization and vegetation degradation across the world's metropolises using DMSP/OLS nighttime light data. *Remote Sensing, 7*(2), 2067–2088. https://doi.org/10.3390/rs70202067

Lu, Y., Coops, N. C., & Hermosilla, T. (2017). Estimating urban vegetation fraction across 25 cities in pan-Pacific using Landsat time series data. *ISPRS Journal of Photogrammetry and Remote Sensing*. https://doi.org/10.1016/j.isprsjprs.2016.12.014

Malek, Ž., & Verburg, P. (2017). Mediterranean land systems: Representing diversity and intensity of complex land systems in a dynamic region. *Landscape and Urban Planning*. https://doi.org/10.1016/j.landurbplan.2017.05.012

Melchiorri, M., Florczyk, A. J., Freire, S., Schiavina, M., Pesaresi, M., & Kemper, T. (2018). Unveiling 25 years of planetary urbanization with remote sensing: Perspectives from the global human settlement layer. *Remote Sensing, 10*(5), 1–19. https://doi.org/10.3390/rs10050768

Oecd. (2020). *Cities in the world: A New Perspective on Urbanisation*. OECD Urban Studies/European Union.

Pesaresi, M., & Freire, S. (2016). *GHS-SMOD R2016A - GHS settlement grid, following the REGIO model 2014 in application to GHSL Landsat and CIESIN GPW v4-multitemporal (1975–1990-2000-2015)*. European Commission Joint Research Centre (JRC).

Potere, D., Schneider, A., Angel, S., & Civco, D. L. (2009). Mapping urban areas on a global scale: Which of the eight maps now available is more accurate? *International Journal of Remote Sensing*. https://doi.org/10.1080/01431160903121134

Sabo, F., Corbane, C., Florczyk, A. J., Ferri, S., Pesaresi, M., & Kemper, T. (2018). Comparison of built-up area maps produced within the global human settlement framework. *Transactions in GIS, 22*(6), 1406–1436. https://doi.org/10.1111/tgis.12480

Shaw, B. J., van Vliet, J., & Verburg, P. H. (2020). The peri-urbanization of Europe: A systematic review of a multifaceted process. *Landscape and Urban Planning*. https://doi.org/10.1016/j.landurbplan.2019.103733

Sun, C., Wu, Z. F., Lv, Z. Q., Yao, N., & Wei, J. B. (2012). Quantifying different types of urban growth and the change dynamic in Guangzhou using multi-temporal remote sensing data. *International Journal of Applied Earth Observation and Geoinformation*. https://doi.org/10.1016/j.jag.2011.12.012

Sun, L., Chen, J., Li, Q., & Huang, D. (2020). Dramatic uneven urbanization of large cities throughout the world in recent decades. *Nature Communications*. https://doi.org/10.1038/s41467-020-19158-1

United Nations. (2018). *World Urbanization Prospects 2018. Department of Economic and Social Affairs. World Population Prospects 2018*.

UN-Habitat. (2021). *Annual Report 2020* (pp. 1–86). UN-Habitat.

Václavík, T., Lautenbach, S., Kuemmerle, T., & Seppelt, R. (2013). Mapping global land system archetypes. *Global Environmental Change, 23*(6), 1637–1647. https://doi.org/10.1016/j.gloenvcha.2013.09.004

van Vliet, J., Eitelberg, D. A., & Verburg, P. H. (2017). A global analysis of land take in cropland areas and production displacement from urbanization. *Global Environmental Change, 43*, 107–115. https://doi.org/10.1016/j.gloenvcha.2017.02.001

van Vliet, J., Verburg, P. H., Grădinaru, S. R., & Hersperger, A. M. (2019). Beyond the urban-rural dichotomy: Towards a more nuanced analysis of changes in built-up land. *Computers, Environment and Urban Systems, 74*(December 2018), 41–49. https://doi.org/10.1016/j.compenvurbsys.2018.12.002

Wang, J., Zhou, W., Pickett, S. T. A., Yu, W., & Li, W. (2019). A multiscale analysis of urbanization effects on ecosystem services supply in an urban megaregion. *Science of the Total Environment*. https://doi.org/10.1016/j.scitotenv.2019.01.260

Wehrens, R., & Kruisselbrink, J. (2018). Flexible self-organizing maps in kohonen 3.0. *Journal of Statistical Software, 87*(7). https://doi.org/10.18637/jss.v087.i07

Xu, G., Zhou, Z., Jiao, L., & Zhao, R. (2020). Compact urban form and expansion pattern slow down the decline in urban densities: A global perspective. *Land Use Policy, 94* (January), Article 104563. https://doi.org/10.1016/j.landusepol.2020.104563

Yang, Y., Xiao, P., Feng, X., & Li, H. (2017). Accuracy assessment of seven global land cover datasets over China. *ISPRS Journal of Photogrammetry and Remote Sensing*. https://doi.org/10.1016/j.isprsjprs.2017.01.016

Yu, W., & Zhou, W. (2017). The spatiotemporal pattern of urban expansion in China: A comparison study of three urban megaregions. *Remote Sensing*. https://doi.org/10.3390/rs9010045

Yu, X. J., & Ng, C. N. (2007). Spatial and temporal dynamics of urban sprawl along two urban-rural transects: A case study of Guangzhou, China. *Landscape and Urban Planning, 79*(1), 96–109. https://doi.org/10.1016/j.landurbplan.2006.03.008

Zhang, W., Randall, M., Jensen, M. B., Brandt, M., Wang, Q., & Fensholt, R. (2021). Socio-economic and climatic changes lead to contrasting global urban vegetation trends. *Global Environmental Change, 71*(October), Article 102385. https://doi.org/10.1016/j.gloenvcha.2021.102385

Zhang, X., Friedl, M. A., Schaaf, C. B., Strahler, A. H., & Liu, Z. (2005). Monitoring the response of vegetation phenology to precipitation in Africa by coupling MODIS and TRMM instruments. *Journal of Geophysical Research D: Atmospheres.*. https://doi.org/10.1029/2004JD005263

Zhao, L., Dai, A., & Dong, B. (2018). Changes in global vegetation activity and its driving factors during 1982–2013. *Agricultural and Forest Meteorology, 249*(October 2016), 198–209. https://doi.org/10.1016/j.agrformet.2017.11.013

Zhong, Y., Lin, A., & Zhou, Z. (2019). Evolution of the pattern of spatial expansion of urban land use in the poyang lake ecological economic zone. *International Journal of Environmental Research and Public Health, 16*(1), 1–14. https://doi.org/10.3390/ijerph16010117